Chapter 7
Terahertz Nanoscale Science and Technology

John W. Bowen

Abstract The terahertz (THz) frequency range, which falls between the infrared and microwave portions of the spectrum, is rich in potential applications because the photon energies involved can open a window on physical and biological processes that are inaccessible to other wavelengths. After an introduction to the terahertz range, some example applications, and the techniques used for the generation, detection and manipulation of terahertz radiation, this chapter concentrates on the latest developments in terahertz nanoscale science and technology. Topics covered include the use of nano-structures to enhance the emission and detection of terahertz radiation; THz quantum cascade lasers; terahertz detection approaching the quantum limit; THz nanoscopy; terahertz scanning tunnelling microscopy (THz-STM); and the use of THz spectroscopy to probe biological function at the molecular level.

Keywords Terahertz technology · Nanoscale devices · Nanoscopy · Biomolecular spectroscopy

7.1 Introduction

The terahertz part of the electromagnetic spectrum, encompassing frequencies be-tween 100 GHz and 10 THz, and corresponding to wavelengths of 30 μm to 3 mm, has important properties that make it attractive for a wide range of application areas. The photon energies correlate with molecular rotations, hydrogen bonding stretches and torsions, bond vibrations and crystalline phonon vibrations, providing spectroscopic information. Furthermore, the conductivity of materials and the ultrafast motion of charge carriers can be probed using terahertz spectroscopy. Many materials that are opaque in other parts of the spectrum transmit terahertz

J. W. Bowen (✉)
School of Biological Sciences, University of Reading, Reading, UK
e-mail: j.bowen@reading.ac.uk

B. Di Bartolo et al. (eds.), *Quantum Nano-Photonics*, NATO Science for Peace and Security Series B: Physics and Biophysics,
https://doi.org/10.1007/978-94-024-1544-5_7

radiation to some degree, enabling depth-resolved imaging of their internal structure. Additionally, thermal emission peaks in this frequency range for temperatures of a few Kelvin or tens of Kelvin, enabling astronomical observation of cool objects in space, as well as of the light from rapidly receding, distant objects at the edge of the universe, which has been red-shifted into the terahertz range. On top of this, the photon energies are insufficient to cause damage to materials or harm to individuals through ionization. These factors have given rise to applications in areas as diverse as astronomy, non-destructive testing, art conservation, medical imaging, pharmacy, atmospheric science, and security screening. Despite the relatively large scale of the wavelengths involved, terahertz technology can benefit from the use of nano-structured devices and from exploiting quantum effects. Astonishingly, it can also provide the means to achieve sub-nanometer scale resolution imaging with simultaneous ultrafast time resolution and to probe biological function at the molecular level.

In order to appreciate these latest developments in terahertz nanoscale science and technology, it is helpful to have some understanding of terahertz systems in general, not just at the nanoscale, and that is where this chapter starts. It then moves on to discuss the use of nano-structures to enhance the generation and detection of terahertz radiation, terahertz quantum cascade lasers, detection approaching the quantum limit, terahertz nanoscopy, terahertz scanning tunneling microscopy, and terahertz biomolecular spectroscopy.

7.2 Terahertz Systems

7.2.1 Time Domain Systems

Many terahertz spectroscopy and imaging systems in current use are based on the generation and detection of short pulses of terahertz radiation. In order to make a spectroscopic measurement, the sample is placed in the terahertz beam so that the pulse is incident upon it and the emergent pulse is recorded as a time domain waveform. The sample will attenuate the pulse, through a combination of absorption, reflection at its surfaces and scattering, and will introduce a time delay as the pulse traverses it, which will act to broaden the width of the pulse if the material is dispersive. Because the terahertz pulse is only a few hundred femtoseconds in length, it contains a broad range of terahertz frequencies, typically spanning from 100 GHz to over 3 THz. Therefore, a complex fast Fourier transform of the time domain waveform produces its frequency domain spectrum. By taking the ratio of the spectrum of the received waveform to that when no sample is in the beam (the reference waveform), the amplitude and phase transmission coefficients at each frequency within the bandwidth may be determined.

This approach can be extended to achieve terahertz imaging by focusing the beam to a small spot at the sample and either moving the sample through the terahertz beam or scanning the beam across the sample. Typically, this is accomplished by mounting either the sample or the generation and detection heads on x–y translation stages, to allow scanning in two dimensions. Therefore, the image data is acquired pixel by pixel and consists of a full time domain waveform for each location of the beam across the sample surface. There are many ways to construct an image from this data. For example, the peak amplitude of the time domain waveform may be plotted for each pixel, or the peak amplitude integrated over different frequency ranges. Each representation can highlight different features of the sample and the most appropriate to use will depend on the application. The resulting images are usually plotted as false colour maps.

Terahertz images and spectra can be acquired in both transmission and reflection geometry by appropriate reconfiguration of the system. In reflection mode, the time domain waveform for a stratified sample will consist of a series of peaks corresponding to reflections from individual layer boundaries. Therefore, an individual peak may be isolated and an image constructed from mapping it across the sample, allowing depth-resolved imaging to be achieved. Alternatively, by stacking time domain waveforms recorded along a line across the sample so that they are side by side, and plotting a false colour map of the amplitude of each time domain point, a cross-sectional image, or B-scan, of the sample can be constructed. Signal processing techniques based on deconvolution can be used to improve the resolution, to the degree that sub-wavelength and sub-pulse width depth resolution is possible [1].

The two commonest techniques for generating the short terahertz pulses used in these systems are photoconductive generation and optoelectronic generation. Both are driven by the pulse from a near-infrared femtosecond laser. In photoconductive generation, the near-infrared laser pulse is incident on a piece of semiconductor at the feed gap between the two halves of a planar dipole antenna, which has been fabricated on a suitable dielectric substrate and is designed for radiation of terahertz frequencies. A potential difference is established between the two halves of the antenna by applying a d.c. bias voltage across them. Initially, with no near-infrared laser pulse present, the semi-conductor is non-conducting and no current flows through the antenna; hence there is no radiation. However, when the laser pulse is incident on the semiconductor, photocarriers are generated and current begins to flow. After the laser pulse has ceased, the photocarriers relax back to the conduction band and the current returns to zero. The burst of current through the antenna results in a radiated pulse of terahertz radiation. Because of the carrier lifetime, the terahertz pulse is longer than that from the near-infrared laser, typically being hundreds rather than tens of femtoseconds in duration, but it still spans frequencies up to around 3 THz.

The alternative technique of optoelectronic generation, replaces the photoconductive antenna with a non-linear crystal of material such as zinc telluride. When the near-infrared laser pulse propagates through the crystal, the non-linearity results in the generation of an emergent pulse at the difference frequencies between the

frequency components of the input pulse. Because the femtosecond input pulse has a broad frequency content spanning several terahertz about its centre frequency in the infrared, the emergent pulse covers a broad range of frequencies in the terahertz part of the spectrum. While this technique produces broader band terahertz pulses than photoconductive detection, it requires use of an amplified laser system to produce the infrared input pulse.

A gated detection system is required in order to resolve the shape of the terahertz pulse after it has interacted with the sample and to record the time domain waveform. Again, there are two detection techniques in common use, both of which use a fraction of the signal split off from the near-infrared femtosecond laser using a beam splitter as the gating or probe signal. This probe signal activates the detector for a length of time dependent on the laser pulse width, which is significantly shorter than the width of the received terahertz pulse. By introducing an optical delay line between the laser pulse which drives the generator, commonly referred to as the pump pulse, and the probe pulse, different portions of the received terahertz pulse can be detected. As the laser produces a series of pulses, each of which generates an identical terahertz pulse, the optical delay line can be scanned so that each successive probe pulse maps out the shape of the received terahertz waveform at the detector over a sequence of received terahertz pulses. This assumes that the sample does not significantly change its properties on this timescale.

Photoconductive detection uses an antenna similar to that used for photoconductive generation. However, in this case, there is no applied bias voltage and the magnitude of the current flowing through the antenna corresponds to the amplitude of the received signal. In the absence of the probe pulse, no current can flow through the antenna, even with an applied terahertz signal. However, while the probe pulse is present, photocarriers are generated in the semiconductor, enabling a current to flow through the antenna, driven by the received terahertz signal.

Alternatively, electro-optic detection utilizes the Pockels effect in an appropriately oriented crystal of a material such as zinc telluride. While no terahertz signal is incident on the crystal, an incident probe pulse from the linearly polarized near infrared laser will be converted to a circularly polarized output pulse, due to birefringence in the crystal. If a terahertz pulse is now applied co-linearly with the probe pulse, its electric field will polarize the crystal and modify its birefringence so that the emergent infrared pulse will be elliptically polarized. The amplitude of the received terahertz signal can be determined by separating the emergent infrared pulse into its orthogonal linearly polarized components, using a quarter wave plate and Wollaston prism, and detecting these with a balanced pair of photodetectors. The terahertz signal amplitude is proportional to the difference in intensities recorded at the two photodetectors.

While these time domain systems work well, there is still a desire to improve the efficiencies of terahertz generation and detection in order to increase signal-to-noise ratios and reduce data acquisition times. Section 7.3 discusses recent developments in this direction based on the use of nanostructures.

7.2.2 Frequency Domain Systems

There are many approaches to the recording of terahertz signals directly in the frequency domain, based on the use of continuous wave rather than pulsed sources. While many of these sources are sufficiently narrow band that they can be considered to produce essentially a single output frequency, some can be swept over a range of frequencies to enable spectroscopic information to be retrieved. Others are inherently broadband noise sources and frequency comb generators, which require frequency selective components or interferometric spectrometers to separate the terahertz signal into its frequency components for spectroscopic purposes.

Of particular note here, are photomixers, which use non-linear devices mounted in terahertz planar antennas to derive a terahertz output at the difference frequency between two diode lasers, which are typically operating at infrared communications wavelengths. The terahertz output frequency can be swept by sweeping the wavelength offset between the two lasers. Similar nanostructure enhancements to those described in Sect. 7.3 for photoconductive emitters and detectors are also applicable in the case of these devices.

Another class of continuous wave sources are terahertz quantum cascade lasers. As their name implies, these exploit quantum effects for their operation. They are discussed more fully in Sect. 7.4.

Quantum effects can also play an important role in terahertz detection, especially of the very small amounts of terahertz radiation received from astronomical bodies. This matter is discussed in Sect. 7.5.

7.2.3 Terahertz Optics

Lenses and mirrors are commonly used within terahertz systems in order to control the divergence and focusing of beams. However, because of the relatively large size of the wavelengths involved, the effects of diffraction cannot be ignored. This has two major consequences. Firstly, geometrical optics cannot be used for the design of terahertz systems, and secondly, there is a limitation on the minimum sized spot to which one can focus the radiation.

Figure 7.1 illustrates the propagation and focusing of a terahertz beam by a lens. Here it is assumed that the beam has a Gaussian transverse amplitude distribution, with the contour lines representing the $1/e$ amplitude level in the beam. It is clear that the beam spreads due to diffraction as it propagates and that the introduction of an optical component, such as the lens, is necessary to refocus the beam and stop it spreading to unmanageable size. The lens focuses the beam to a minimum-sized spot, known as the beam-waist, beyond which it spreads again at the same rate with which it converged. Thus a series of lenses or focusing mirrors spaced one after the other is necessary to constrain the spread of the beam within a given off-axis diameter.

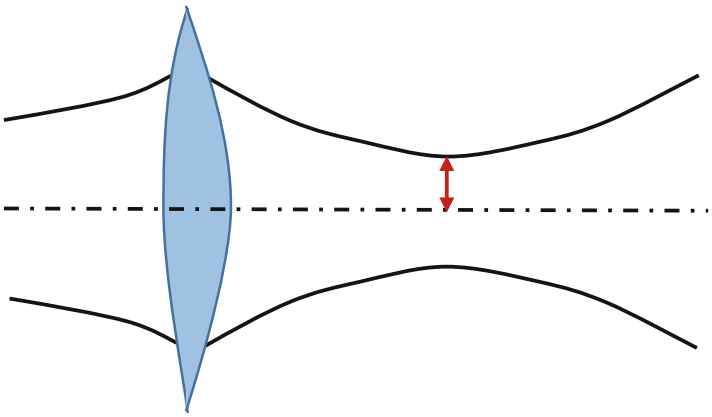

Fig. 7.1 Propagation and focusing of a terahertz beam by a lens. The solid black lines represent the 1/e amplitude contours in the beam. The dash-dot line is the optic axis. The red arrow indicates the beam-waist location

The severity of the diffraction is due to practical constraints on the size of systems, which limit the lenses and mirrors to typically only a few tens of wavelengths in diameter. Furthermore, in order to maintain the beam within that diameter, the lenses and mirrors have to be placed within the near to far field transition region of the beam, and the changing curvature of the phase-fronts at different points along the beam must be taken into account in the design of their surface profiles.

Beams with a transverse amplitude distribution which is other than Gaussian may be described by a superposition of Hermite-Gaussian or Laguerre-Gaussian beam-modes, as long as the beam can be considered paraxial. While the spreading of each of these beam-modes occurs at the same rate as the fundamental Gaussian beam-mode, they slip in phase relative to each other as they propagate, so that the resultant superposition can show a complicated changing form at different points along the beam. Fourier Optics and the angular spectrum of plane waves representation are further tools that can aid in the design of terahertz optical systems, and more details on all of these aspects are covered in [2].

Of particular concern here, is the size of the smallest spot to which the beam can be focused, as that limits the spatial resolution in conventional time domain imaging. Even with a severely non-paraxial beam, diffraction limits the minimum beam-waist size to around half a wavelength. Given the wavelengths involved, this is clearly insufficient to achieve nanoscale resolution. Ways to overcome this, which can deliver orders of magnitude improvement in spatial resolution are described in Sects. 7.6 and 7.7. Furthermore, Sect. 7.8 shows how it is possible to use terahertz spectroscopy to investigate nanoscale phenomena in biological systems, without the need to focus the beam to nanoscale dimensions.

7.3 Nanostructure Enhancement of Sources and Detectors

7.3.1 Enhancement of Photoconductive Emitters, Detectors and Photomixers

In a conventional photoconductive emitter, the size of the antenna feed gap is designed to match the diffraction limited spot size of the near infrared pump laser. However, because of the drift velocity of the photocarriers, only a small number of them reach the metal contact electrodes of the antenna on a sub-picosecond timescale that is fast enough to contribute to the terahertz pulse. Any photocarriers generated further than about 100 nm from the contact electrodes do not contribute. Often, short carrier lifetime semiconductors are used to ensure that any remaining photocarriers recombine rather than contribute to a dc current that acts to lower the bias field, which reduces the carrier acceleration between the electrodes.

However, the introduction of three-dimensional nanoscale contact electrodes in the antenna feed gap has enabled a record 7.5% optical-to-terahertz power conversion efficiency to be achieved [3]. The contact electrodes take the form of gratings of V-shaped groves cutting into the surface of the low temperature GaAs semiconductor. The grooves have metallized side-walls and are spaced apart so that the intervening regions of GaAs taper from a width of 100 nm at the surface of the GaAs slab to 160 nm over the 400 nm depth of the grooves. Thus, this structure forms an array of sub-wavelength slab waveguides for the 800 nm wavelength pump laser beam. Both of the anode and cathode contact electrodes consist of a 15 μm $\times$ 15 μm area of these gratings. The two electrodes are spaced apart by 5 μm and are connected to the arms of a logarithmic spiral terahertz antenna.

Although the slab waveguides have a sub-wavelength height, the grating structure excites surface waves that enable efficient coupling of the incident infrared laser beam into the TEM waveguide modes. The coupling is further enhanced by a 200 nm-thick SiO_2 anti-reflection coating deposited over the surface of the nanostructure gratings.

The use of these high aspect ratio grating structures results in a much larger number of photocarriers being generated within 100 nm of the contact electrodes than in conventional photoconductive emitters, and thus an increase in the number of photocarriers that can contribute to terahertz emission. This brings about a significant improvement in optical-to-terahertz conversion efficiency. The depth of the grooves in the grating structure is important because, although improvements in efficiency were seen in earlier work utilizing two-dimensional plasmonic gratings on the semiconductor surface [4], they were unable to exploit the photocarriers generated deeper within the semiconductor.

While the work described above has focused on improving photoconductive generation, similar antenna structures are used for photoconductive detectors and in photomixers, and so the use of nanostructured electrodes of a similar type should result in improvements in their efficiency too.

7.3.2 *Terahertz Generation from Plasmonic Nanoparticle and Nanohole Arrays*

Recently, there has been much interest in the emission of terahertz radiation observed when metallic nanostructures are illuminated by femtosecond infrared laser pulses, as it could prove the basis of a useful terahertz source. There has been some controversy over the mechanism involved, as different power law dependencies of the emitted terahertz intensity on the incident infrared intensity have been observed in experiments carried out by different teams, indicating different potential emission mechanisms. However, recent experiments by Polyushkin et al. [5] on plasmonic nanoparticle and nanohole arrays indicate that there are two different regimes involved.

At lower incident infrared intensities, the terahertz emission shows a slightly less than second order dependence, suggesting that the emission is due to optical rectification. At higher incident intensities, a fourth to fifth order dependence is seen, which is consistent with ejection of photo-electrons from the metal surface, caused by plasmon enhancement and multi-photon absorption of the infrared radiation, followed by pondermotive acceleration of the emitted electrons in the high electric field gradients that exist close to the metal surface due to the plasmonic enhancement, giving rise to the terahertz emission. The results presented in [5] were the first to show both regimes in the same experiment and were backed up by electron emission measurements using a time-of-flight electron spectrometer, which showed good correlation with the terahertz emission results, supporting the proposed emission mechanisms. A third regime with much reduced power dependence was seen at even higher incident intensities, which is thought to be due to the onset of tunnel ionization rather than multiphoton ionization.

It is clear that the emission depends on the local field enhancement specific to the nanostructures used. In [5], the nanoparticle arrays were designed to produce a strong plasmonic field enhancement at the incident laser wavelength and were found to have terahertz emission consistent with multiphoton ionization, but not optical rectification, within the range of incident laser intensities possible within the experimental setup. The nanohole arrays, on the other hand, were designed to have a lower field enhancement, and showed a clear transition between the optical rectification and multiphoton ionization regimes. Both samples showed the onset of tunnel ionization at very high incident intensities.

7.4 Terahertz Quantum Cascade Lasers

Conventional laser diodes, based on interband transitions between the conduction and valance bands in semiconductors, are limited to the visible and infrared portions of the spectrum, because the bandgap energy, which is of the order of electron-volts, is too high for terahertz emission. However, by exploiting intersubband

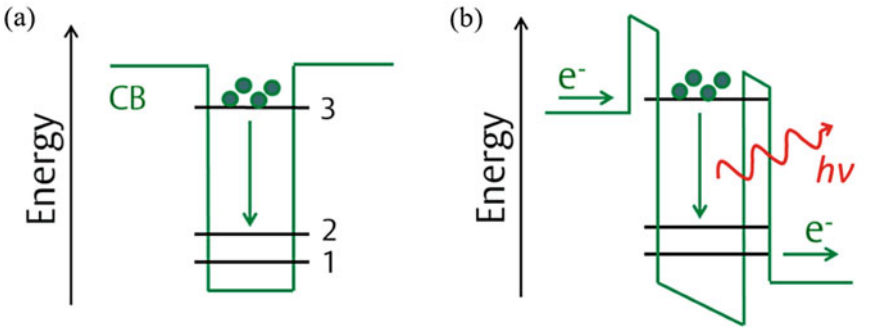

Fig. 7.2 Conduction band (CB) energy levels within a quantum well, (**a**) under zero bias. (**b**) In quantum well between two potential barriers, with applied electric field

transitions in quantum wells, with energies of milli-electron-volts, it is possible to make quantum cascade lasers operating in the terahertz range. These compact semiconductor devices are unipolar, because the emission mechanism only involves electrons, rather than electrons and holes as in interband laser diodes. Therefore, the lasing transitions occur within the conduction band. Moreover, the transition energy is dependent on the thickness of the atomic layers forming the quantum wells, and can be freely adjusted to provide a desired output frequency through bandstructure engineering.

Figure 7.2a shows three energy levels within a quantum well. For lasing to occur, it is necessary to maintain a population inversion between levels 3 and 2. Figure 7.2b shows such a quantum well formed between two potential barriers, under an applied bias voltage. Under the influence of the resulting electric field, electrons tunnel through the potential barrier into level 3, with the lasing transition occurring down to level 2. This lower state is quickly depopulated to level 1, maintaining the population inversion, with the electrons tunneling out of the quantum well through the second potential barrier.

In practical quantum cascade laser designs, multiple quantum wells separated by potential barriers are fabricated next to each other to form superlattices, in which the single well quantum states couple together to form minibands separated by a minigap [6]. This structure forms the active region of the quantum cascade laser, with the lasing transition occurring between the minibands. By cascading a series of these active regions together (typically 100 or more), with intervening injector regions which collect electrons from the lower miniband in one active region and inject them into the upper miniband in the next, each electron can produce multiple lasing transitions as it passes through the device.

In order to confine the radiation within the laser and form the laser cavity, the entire active region cascade structure forms part of a waveguide. Two types of waveguide are in use. In surface plasmon or single metal waveguides, the active region forms a ridge separated by a thin, heavily doped layer from a semi-insulating GaAs substrate, and capped with a metal contact layer. A second metal contact,

adjacent to the ridge that forms the waveguide, enables application of the necessary bias voltage. In this type of waveguide, the radiation is confined as a surface plasmon mode.

In the second type of waveguide, the metal-metal waveguide, the active region forms a ridge sandwiched between a metal layer on the surface of a substrate and second metal contact, with which it is capped. The metal-metal waveguide is better for higher temperature operation of the quantum cascade laser and for achieving operation at lower frequencies. However, it produces lower output power and, because of its tighter field confinement, gives a poorer beam profile [6].

While quantum cascade lasers are well established in the mid-infrared part of the spectrum, their realization at terahertz frequencies has been much more challenging. In part, this has been due to the challenge of developing low-loss waveguides suitable for terahertz frequencies, but also because of the difficulty in achieving population inversion for such small subband spacings. The latter requires the selective injection of electrons into the upper state and not the lower state, as well as an active region design that selectively depopulates the lower state without reducing the population of the upper state. Nevertheless, these difficulties have been overcome sufficiently for terahertz quantum cascade lasers to become available as commercial products.

Performance has been demonstrated at frequencies between 1.2–5 THz and with powers greater than 100 mW in continuous wave mode and greater than 1 W when pulsed. While tuning is limited, tuning over a 330 GHz range centred on 4 THz has been demonstrated using a micro-electromechanical plunger [7]. The greatest practical performance limitation is that of operating temperature, as the maximum operating temperature achieved is currently 199.5 K for pulsed operation and 129 K in continuous wave mode. This is primarily a consequence of thermally activated relaxation between the upper and lower radiative states based on the emission of optical phonons [8]. Alternatives to the GaAs/AlGaAs material system usually used for quantum cascade lasers are being explored, with a view to increasing the maximum operating temperature. The design of the active region is another important factor in this regard.

An alternative approach to achieving room temperature operation, is to make use of intracavity difference frequency generation in dual-wavelength mid-infrared quantum cascade lasers [9]. However, the power output from these devices is more limited, with 2 mW having been achieved in pulsed operation.

There is much current interest in producing broad-bandwidth emission from quantum cascade lasers through the generation of frequency combs. By combining four different active regions with different centre frequencies within a single laser cavity, an instantaneous bandwidth of almost 2 THz has been demonstrated, with peak power up to 10 mW in pulsed operation [10].

An alternative approach to producing broadband emission, whilst simultaneously producing a more directed beam, is the so-called random laser [11]. In this device, the laser cavity is in the form of a disc of the semiconductor layers on a metalized substrate, capped by a metal layer. The metal layers act as a metal-metal waveguide. Holes with diameter comparable to the emission wavelength are etched through

the upper metal contact and entire semiconductor structure in a random pattern. While the radiation is confined between the metal plates, it can travel in any in-plane direction and encounter the randomly placed holes, which will define the modes of the laser cavity. The holes also serve to couple the radiation out of the cavity. Because the holes are spread across the upper surface of the disc, which covers a much larger area than the end facet of a conventional quantum cascade laser waveguide, the resulting output beam is less divergent and is emitted in a direction normal to the top surface of the device. The result is a comb of frequencies, with spectral content dependent on the laser modes that are excited, and a well-directed beam.

Another recent development is the demonstration of high-resolution gas spectroscopy by self-mixing interferometry [12]. In this case, the beam from a quantum cascade laser passes through a gas cell before encountering a mirror which reflects the beam back though the gas cell to the laser, thus producing external cavity feedback. Tuning the frequency of the quantum cascade laser across a gas absorption line reduces the external feedback, which can be detected by monitoring the voltage across the laser.

7.5 Detection Approaching the Quantum Limit

The fundamental limit of detection of electromagnetic radiation of any wavelength corresponds to the detection of a single photon within the measurement interval. This is known as the quantum limit [13]. The measurement interval is related to the response time of the detection system. If the bandwidth of a given detection system is $\Delta\nu$, the corresponding measurement time will be $\Delta\nu^{-1}$. Therefore, detection of a single photon within this time, of energy $h\nu$, corresponds to a received signal power

$$P = h\nu \cdot \Delta\nu \tag{7.1}$$

Obviously, for the detection of weak sources of radiation, such as from faint astronomical objects in distant regions of the Universe, it is advantageous to have detection systems that come as close to the quantum limit as possible. While some terahertz detection systems are based on direct detection using broadband thermal detectors, others are based on heterodyne detection. The latter have the advantage of retaining all of the phase and frequency present in the input signal. They operate by diplexing the incoming signal with the signal from a local oscillator, which forms part of the detection system, or receiver, and applying this combined signal to a non-linear device known as a mixer. The output from the mixer is at the difference frequency between the input signal and that of the local oscillator. If a range of frequencies is present at the input, the result will be a range of frequencies present at the output, with the incoming signal spectrum downconverted from the terahertz range to much lower frequencies, which can be handled by conventional electronics. Inevitably, there will be noise in the detection system that will limit the smallest

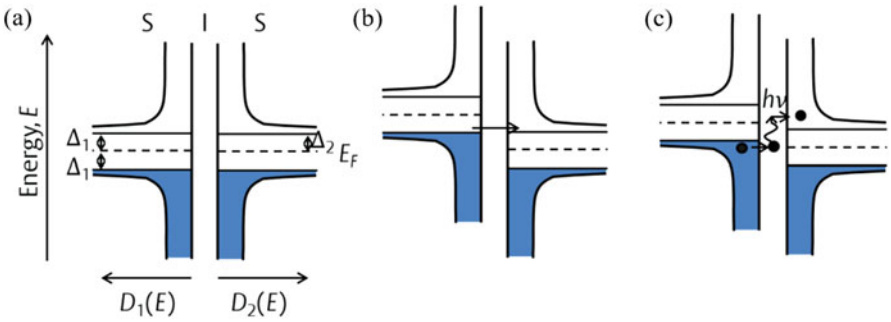

Fig. 7.3 SIS tunnel junction under different bias conditions. (**a**) Under zero bias. (**b**) Biased such that $eV_b = \Delta_1 + \Delta_2$, allowing quasiparticle tunneling. (**c**) Biased such that $eV_b = \Delta_1 + \Delta_2 - h\nu$, allowing photon-assisted tunneling

signal it can detect. In heterodyne systems, this is conventionally represented by a mixer noise temperature T_m, related to this least detectable signal power by

$$P = kT_m\Delta\nu \tag{7.2}$$

where k is Boltzmann's constant. Thus, equating (7.1) and (7.2) gives the quantum limit in terms of mixer noise temperature as

$$T_m = h\nu/k \tag{7.3}$$

Fortunately, it is possibleto approach the quantum limit in heterodyne detection at frequencies up to about 1 THz by using superconductor-insulator-superconductor tunnel junctions as mixers. These SIS mixers consist of two superconductor regions separated by a thin insulator barrier, of the order of 0.06–0.2 nm in thickness. The device is operated well below the superconducting transition temperature. The situation under different bias conditions is illustrated in Fig. 7.3. The figure represents energy on the vertical axis and density of states in the superconductors on the horizontal axis. The blue shaded regions indicate filled states, whereas unshaded regions are empty. In a superconductor, there exists a superconducting energy gap of height 2Δ, centred on the Fermi energy E_F. If different superconductors are used on either side of the insulating barrier, they will have different energy gaps, indicated in Fig. 7.3 by Δ_1 and Δ_2. Under zero bias (Fig. 7.3a), no tunneling occurs across the junction. If the bias is increased such that $eV_b > \Delta_1 + \Delta_2$, where e is the electronic charge and V_b is the bias voltage, filled states on one side of the junction line up with empty states on the other side and there is sufficient energy for Cooper pairs to break up and the resulting quasiparticles to tunnel across the junction (Fig. 7.3b). This results in a very rapid onset of current when $eV_b = \Delta_1 + \Delta_2$ because of the very large density of states close to the superconducting energy gap edge on either side of the junction. If the bias voltage is such that $eV_b < \Delta_1 + \Delta_2$, the additional

energy required for tunneling can be provided by an incoming photon (Fig. 7.3c). The resulting extreme non-linearity in response to incident radiation is the reason that SIS mixers have a performance that approaches the quantum limit.

The use of SIS mixers is now well established in terahertz astronomy. For example, SIS mixers are used in the receivers for the Atacama Large Millimeter/Submillimeter Array (ALMA), which operates at frequencies from 30 GHz – 1 THz. A receiver noise temperature corresponding to about three times the quantum limit has been achieved in the ALMA 787–950 GHz band [14].

7.6 Terahertz Nanoscopy

A number of approaches are being explored to enable sub-wavelength terahertz imaging, including the use of sub-wavelength apertures and tapered plasmonic waveguides. However, the most impressive results to date have been achieved by applying a terahertz beam to the tip of an atomic force microscope hovering over the sample to be imaged. The microscope tip acts as an antenna to concentrate the terahertz fields, with the scattered field being dependent on interaction of the evanescent field with the sample. Because of non-linearity in the field near the pointed end of the microscope tip, the scattered field contains higher harmonics of the incident terahertz frequency, which can be separated using a Michelson interferometer, enabling the scattered radiation to be distinguished from the incident radiation. Using a 2.54 THz continuous wave beam, Huber et al. [15] have demonstrated 40 nm spatial resolution imaging of nano-transistors using this technique, corresponding to a resolution of 1/3000 of the wavelength. They found that it was possible to image regions of different carrier density within single nano-transistors. Current efforts are directed towards improving the technique by replacing the atomic force microscope tip with a tip specifically designed to act as a terahertz antenna.

7.7 Terahertz Scanning Tunneling Microscopy (THz-STM)

Even finer spatial resolution is possible with THz-STM, although, in this case, the terahertz signal is used to enable ultrafast time resolution in scanning tunneling microscopy, rather than to record terahertz images directly. An incident terahertz pulse acts to provide an ultrafast modulation to the bias voltage in a scanning tunneling microscope (STM), inducing tunneling of electrons between the sample and scanning tip on a sub-picosecond timescale. This is achieved without modification to the STM, by focusing the terahertz beam so that it couples to the scanning tip of the STM, which acts as an antenna for the terahertz radiation. The non-linear current-voltage characteristic of the sample-tip tunnel junction rectifies the resulting time-dependent tunnel current, enabling it to be detected with the conventional STM electronics. In the initial demonstration of the technique [16], electron trapping in an

InAs nanodot, induced by an 800 nm optical pump pulse, was imaged in an optical pump-terahertz probe experiment. A time resolution of below 500 fs was achieved simultaneously with a 2 nm spatial resolution, corresponding to 1/150,000 of the terahertz wavelength.

Since then, the technique has been improved to the extent that it is now possible to produce a slow motion movie of the ultrafast motion of a single molecular orbital, with a spatial resolution of 0.6 Å and a time resolution of 115 fs [17]. This was demonstrated by imaging pentacene molecules, which were electronically decoupled from an underlying metal substrate by a monolayer of NaCl. Appropriate choice of the terahertz pulse amplitude opens an otherwise forbidden tunneling channel through the highest occupied molecular orbital (HOMO), enabling an electron to tunnel from the HOMO to the STM tip, and a further electron to tunnel from the metal substrate into the HOMO, resulting in a detectable ultrafast tunnel current. Removal of the electron from the HOMO abruptly changes the Coulomb and van der Waals forces between the molecule and the substrate, setting the molecule into oscillatory motion. By using an initial terahertz pulse to act as a pump to set the molecule into motion, and following it after a delay with a second terahertz pulse to act as a probe, the oscillation can be mapped out for different time delays between pairs of pump and probe pulses. The oscillation can be detected because variation of the spacing between the molecule and the scanning tip modulates the tunnel current. In the case of pentacene over a gold substrate, a 0.5 THz oscillation was observed, with an amplitude corresponding to ± 4 pm. Use of a different molecule (copper phtalocyanine) or modification of the substrate was seen to produce different oscillation frequencies, due to the dependence on the forces between the molecule and substrate. Furthermore, by appropriate choice of substrate and terahertz pulse amplitude, it is possible to selectively image the lowest unoccupied molecular orbital (LUMO) rather than the HOMO. This technique opens up new possibilities for studying the quantum motion of molecules on femtosecond timescales and with single electronic orbital resolution.

7.8 Biomolecular Spectroscopy

To gain a full understanding of the function of biomolecules, such as proteins, it is important to consider not just the molecule itself, but also the network of water molecules that surround it in a biological system. Terahertz spectroscopy can provide unique information in this regard, complementary to that provided by other techniques, as both the collective vibrational modes of biomolecules and dynamic changes in the water network that occur on sub-picosecond timescales are accessible to it. By measuring the terahertz absorption of solutions of biomolecules as a function of concentration, it has been deduced that biomolecules slow the fluctuations in the hydrogen bond network of the water molecules in their vicinity, producing a surrounding shell of hydration water with modified dynamics and

a distinct terahertz absorbance [18]. This behavior is consistent with molecular dynamics simulations, which show a shift in the vibrational density of states of the hydration water towards higher frequencies, resulting in increased absorption above about 1.5 THz and decreased absorption below this frequency [19]. Furthermore, from the profile of the absorption versus concentration curve, it is possible to determine the point at which the dynamic hydration shells begin to overlap, and thus deduce their size. In the case of proteins, it has been found that their influence on the water dynamics extends as far away as at least 10 Å; and to greater than 20 Å in some cases [18]. This is a much greater distance than had been previously assumed, based on experiments carried out using other techniques, which are insensitive to water fluctuations on the sub-picosecond timescale. Consequently, because of the separations between molecules in live cells, much of the water can be in this altered dynamic state.

Thus, because of the strong interaction between biomolecules and their surrounding water network, it is possible to make inferences about the state of the biomolecule by measuring the terahertz absorption, which tends to be dominated by the water. For example, it is possible to detect changes in molecular conformation and the presence of site-specific mutants. Terahertz spectroscopy of antifreeze proteins, which enable some animals to survive in sub-freezing temperatures by binding to nano-sized ice crystals, restricting their further growth, has suggested the existence of a gradient of hydrogen bond dynamics towards the bond site. This hydration funnel is thought to provide a long-range interaction targeting the antifreeze protein towards the ice crystal, eventually enabling it to bond to its surface through a local, short-range interaction at the antifreeze protein's ice-binding site [19]. Further terahertz measurements have indicated that a hydration funnel may play an equivalent role in enzyme-substrate catalysis [19].

Similarly, terahertz spectroscopy shows great promise for label-free detection in biomedical applications. For example, it has been demonstrated that changes in the terahertz absorption of solvation water can be used to enable the label-free detection of antibody-antigen binding in estrogen receptor alpha, which is an important biomarker for breast cancer diagnosis [20].

7.9 Conclusions

This chapter has shown how terahertz radiation can be used to provide information on nanoscale phenomena inaccessible through other means, as well as how nanoscale technology can be used to improve the performance of terahertz systems in general. This is despite the relatively long wavelengths involved. Indeed, proportionally speaking, the spatial resolution that has been achieved surpasses that in any other part of the electromagnetic spectrum. Terahertz science and technology is a relatively young field, due to the technological challenges of operating in this part of the spectrum. Nevertheless, terahertz technology has advanced dramatically in recent years and it is anticipated that new applications that make use of the unique characteristics of terahertz radiation will continue to emerge in the future.

References

1. Walker GC, Bowen JW, Labaune J, Jackson J-B, Hadjiloucas S, Roberts J, Mourou G, Menu M (2012) Terahertz deconvolution. Opt Express 20(25):27230–27241
2. Martin DH, Bowen JW (1993) Long-wave optics. IEEE Trans Microw Theory Tech 41(10):1676–1690
3. Yang S-H, Hashemi MR, Berry CW, Jarrahi M (2014) 7.5% optical-to-terahertz convesion efficiency offered by photoconductive emitters with three-dimensional plasmonic contact electrodes. IEEE Trans Terahertz Sci Tech 4(5):575–581
4. Berry CW, Jarrahi M (2012) Terahertz generation using plasmonic photoconductive gratings. New J Phys 14:105029
5. Polyushkin DK, Márton I, Rácz P, Dombi P, Hendry E, Barnes WL (2014) Mechanisms of THz generation from silver nanoparticle and nanohole arrays illuminated by 100 fs pulses of infrared light. Phys Rev B 89:125426
6. Williams BS (2007) Terahertz quantum-cascade lasers. Nat Photonics 1(9):517–525
7. Qin Q, Reno JL, Hu Q (2011) MEMS-based tunable terahertz wire-laser over 330 GHz. Opt Lett 36(5):692–694
8. Vitiello MS, Scalari G, Williams B, De Natale P (2015) Quantum cascade lasers: 20 years of challenges. Opt Express 23(4):5167–5182
9. Belkin MA, Capasso F (2015) New frontiers in quantum cascade lasers: high performance room temperature terahertz sources. Phys Scr 90:118002
10. Rösch M, Scalari G, Beck M, Süess MJ, Bachmann D, Unterrainer K, Darmo J, Faist J (2017) Terahertz quantum cascade laser based frequency comb with 1 THz spectral bandwidth and dual-comb operation. In: OTST 2017 optical terahertz science and technology abstract book. Institute of Physics, London
11. Schönhuber S, Brandstetter M, Hisch T, Deutsch C, Krall M, Detz H, Andrews AM, Strasser G, Rotter S, Unterrainer K (2016) Random lasers for broadband directional emission. Optica 3(10):1035–1038
12. Hagelschuer T, Wienold M, Richter H, Schrottke L, Biermann K, Grahn HT, Hübers H-W (2016) Terahertz gas spectroscopy through self-mixing in a quantum-cascade laser. Appl Phys Lett 109(19):191101
13. Tucker JR, Feldman MJ (1985) Quantum detection at millimetre wavelengths. Rev Mod Phys 57(4):1055–1114
14. Uzawa Y, Fujii Y, Kroug M, Makise K, Gonzalez A, Kaneko K, Kojima T, Miyachi A, Saito S, Terai H, Wang Z (2016) Development of superconducting THz receivers for radio astronomy. In: Proceedings of 41st international conference on infrared, millimeter and terahertz waves IRMMW-THz 2016, H3A.5. IEEE, Copenhagen
15. Huber AJ, Keilmann F, Wittborn J, Aizpurua J, Hillenbrand R (2008) Terahertz near-field nanoscopy of mobile carriers in single semiconductor nanodevices. Nano Lett 8(11):3766–3770
16. Cocker TL, Jelic V, Gupta M, Molesky SJ, Burgess JAJ, De Los Reyes G, Titova LV, Tsui YY, Freeman MR, Hegmann FA (2013) An ultrafast terahertz scanning tunnelling microscope. Nat Photonics 7(8):620–625
17. Cocker TL, Peller D, Yu P, Repp J, Huber R (2016) Tracking the ultrafast motion of a single molecule by femtosecond orbital imaging. Nature 539(7628):263–267
18. Leitner DM, Gruebele M, Havenith M (2008) Solvation dynamics of biomolecules: modeling and terahertz experiments. HFSP J 2(6):314–323
19. Nibali VC, Havenith M (2014) New insights into the role of water in biological function: studying solvated biomolecules using terahertz absorption spectroscopy in conjunction with molecular dynamics simulations. J Am Chem Soc 136(37):12800–12807
20. Li M, Chang T, Wei D, Tang M, Yan S, Du C, Cui H-L (2017) Label-free detection of anti-estrogen receptor alpha and its binding with estrogen receptor peptide alpha by terahertz spectroscopy. RSC Adv 7(39):24338–24344